

Review

## Enriching the Symmetry of Maxwell Equations through Unprecedented Magnetic Responses of Artificial Metamaterials and Their Revolutionary Applications

Yueh-Chun Lai<sup>1</sup>, Cheng-Kuang Chen<sup>1</sup>, Tsung-Yu Huang<sup>1</sup>, Ieng-Wai Un<sup>1</sup>, Yu-Hang Yang<sup>1</sup> and Ta-Jen Yen<sup>1,2,\*</sup>

<sup>1</sup> Department of Materials Science and Engineering, National Tsing Hua University, Hsinchu 30013, Taiwan; E-Mails: d9531577@oz.nthu.edu.tw (Y.-C.L.); d943569@oz.nthu.edu.tw (C.-K.C.); u930530@oz.nthu.edu.tw (T.-Y.H.); u940561@oz.nthu.edu.tw (I.-W.U.); d943563@oz.nthu.edu.tw (Y.-H.Y.)

<sup>2</sup> Institute of NanoEngineering and MicroSystems, National Tsing Hua University, Hsinchu 30013, Taiwan

\* Author to whom correspondence should be addressed; E-Mail: tjyen@mx.nthu.edu.tw; Tel.: +886-3-5742174; Fax: +886-3-5722366.

Received: 17 May 2011; in revised form: 24 May 2011 / Accepted: 26 May 2011 /

Published: 3 June 2011

---

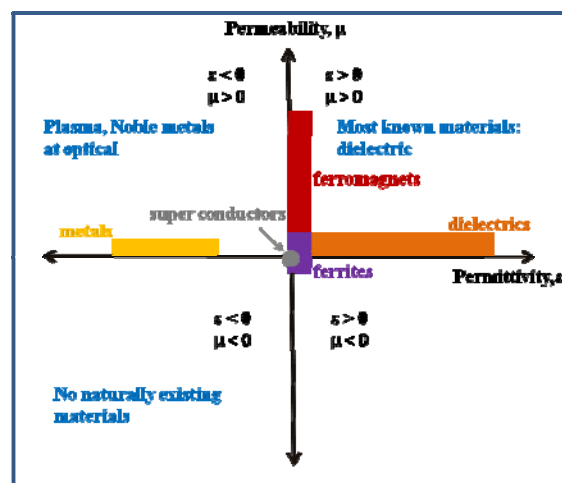
**Abstract:** The major issue regarding magnetic response in nature—“negative values for the permeability  $\mu$  of material parameters, especially in terahertz or optical region” makes the electromagnetic properties of natural materials asymmetric. Recently, research in metamaterials has grown in significance because these artificial materials can demonstrate special and, indeed, extraordinary electromagnetic phenomena such as the inverse of Snell’s law and novel applications. A critical topic in metamaterials is the artificial negative magnetic response, which can be designed in the higher frequency regime (from microwave to optical range). Artificial magnetism illustrates new physics and new applications, which have been demonstrated over the past few years. In this review, we present recent developments in research on artificial magnetic metamaterials including split-ring resonator structures, sandwich structures, and high permittivity-based dielectric composites. Engineering applications such as invisibility cloaking, negative refractive index medium, and slowing light fall into this category. We also discuss the possibility that metamaterials can be suitable for realizing new and exotic electromagnetic properties.

**Keywords:** metamaterials; microwaves; optics; resonance; left-handed materials

## 1. Introduction and Background

As nanotechnology has gradually developed, the interactions between matter and light or EM waves have become more and more significant. The range of electromagnetic material responses found in nature represent only a small subset of that which is theoretically possible. This curious fact is because Maxwell equations are symmetric and scalable but the properties of materials are not. For example, Figure 1 shows four combinations of parameters of materials (*i.e.*, electric permittivity,  $\epsilon$ , and magnetic permeability,  $\mu$ ) and each quadrant represents different physical phenomena. Most known materials, such as dielectrics, exhibit positive  $\epsilon$  and  $\mu$  simultaneously, and metals show negative  $\epsilon$  as depicted in the second quadrant. Nonetheless, we cannot find positive  $\epsilon$  for noble metals, such as silver, gold and copper, as frequencies are lower than ultraviolet ranges. Meanwhile, another intrinsic limitation fetters the magnetic responses of materials. Due to a lack of magnetic monopoles, it is true that magnetic responses are usually rare and weak, particularly in higher frequency ranges. Consequently, magnetic responses from naturally existing materials start to tail off when the frequency of the excited field surpasses 100 GHz or an even lower region.

**Figure 1.** The parameter space of naturally existing materials for their electric permittivity,  $\epsilon$ , and magnetic permeability,  $\mu$ . Notice that no natural material exists in the third and fourth quadrants owing to the lack of negative magnetic permeability except that some ferrites show negative permeability at resonances in the GHz region.



From a microscopic point of view, the aforementioned consequence takes place because magnetic domains inside a given material cannot change their preferred orientation to promptly echo the excited field. Furthermore, it is extremely rare for naturally existing materials to present negative  $\mu$ , especially in high frequency domains—some ferrites indeed show negative permeability at resonances as pinpointed in the lower part of Figure 1, but the frequency is as low as in the GHz region [1,2]. In fact, these intrinsic physical limitations impose immeasurable restrictions on the efforts of scientists and system designers.

The research effort to find magnetic charges in relation to experimental evidence of a natural material's existence is currently a work in progress. The lack of negative permeability ( $-\mu$ ) in natural materials is surmountable by means of "artificial subwavelength periodicity structures" or so-called metamaterials that supply researchers with materials whose properties do not exist in natural materials.

In just the last few years, comprehensive research achievements in metamaterials have raised interest in topics ranging from microwaves to optics. Many fascinating physical phenomena such as negative refractive index medium (NRIM), inverse Doppler effects, and Cerenkov radiation [3–6], and novel applications such as the superlensing effect in breaking diffraction limits [7–10], invisibility cloaking, tunable switch devices, and trapped rainbow light [11–14] have been realized from these microstructured materials. In fact, the NRIM concept was first proposed four decades ago by Veselago [15], but this concept, as originally proposed, has acquired a reputation for being scientific "fiction" because negative  $\epsilon_r$  is realizable in relation to metallic structures whereas negative  $\mu_r$  is absent from nature.

Obtaining negative values for the permeability  $\mu$  is an essentiality to realize negative index metamaterials, but also a novel and intriguing feature, especially in the optical region. It has been shown that negative permeability can be accomplished through a variety of approaches: for instance, inductive patterns such as split-ring resonators as first proposed by Pendry [16], circuit loops connected to microelectronics [17], Swiss rolls [18], pairs of conducting elements called sandwich structures [19,20], high permittivity-based dielectric composites [21], and many others [22,23]. In these fields, researchers should craft intuitive representations identifying the factors that make possess negative permeability in a given frequency range, and also, researchers should compute the value of permeability according to so-called retrieval procedures within these artificial magnetic structures [24–26]. Magnetic metamaterials composed of resonant elements have developed into an important branch of metamaterials research. The key to realizing electromagnetic metamaterials is to construct artificial magnetic moments. In contrast to magnetic and electric dipole moments in natural materials, artificial dipoles can be achieved by distinct designs of LC-resonance, mainly metallic structures. Despite the conventional LC-resonance interpretation for metallic metamaterials, researchers often use the Mie theory as the supporting mechanism for metamaterials instead.

In Section 2 of this review, we will summarize contributions that have guided the field of metamaterials in general and that have promoted magnetic metamaterials research in particular. In the same section, we will discuss, in detail, certain kinds of artificial magnetic structures, their mechanisms, and combinations of artificial electric metamaterials relative to the generation of negative refractive index medium. In Section 3, we will present some special applications corresponding to artificial magnetic responses and negative refractive index metamaterials. These comprise magnetic walls, magnetic surface plasmon resonance, invisible cloaks, artificial electromagnetically induced transparency, and the deceleration of light through metamaterials. Finally, Section 4 will present conclusions and prospects.

## 2. Enriching Magnetic Responses by Artificial Magnetic Metamaterials

Artificial magnetic metamaterials whose compositions are resonant elements are currently flourishing as a topic in metamaterials research. Many magnetic elements have been designed to

possess a strong magnetic response. In this section, we will review some famous and novel magnetic metamaterials: namely, split-ring resonators, sandwich structures, and high permittivity-based dielectric composites. Specifically, we will describe in detail their development and mechanisms.

### 2.1. Split-Ring Resonators

Metamaterials have unprecedented electromagnetic properties through a substitution of artificially constructed meta-atoms for naturally existing atoms. Among diverse metamaterials, the favorite element is the split-ring resonator (SRR) structure whose pioneering design, proposed by Pendry *et al.*, makes use of magnetic meta-atoms to achieve negative magnetic permeability [16]. Wiltshire *et al.* employed this magnetic metamaterials to guide RF flux to the receiver coil, permitting a clear image to be obtained where none might otherwise be detectable [18]. The original double-ring SRRs consist of two concentrated metallic rings as the inductance in series with the capacitance corresponding to two splits opposite each other within the rings, as shown in Figure 2. Another variation, the cut-wire pairs, was proposed in [27], and a three-dimensional isotropic split ring resonator was reported in [28]. It is not necessary to have a double-ring SRR, which characterized many past simulations and experiments seeking to obtain magnetic resonance.

The magnetic dipole is always defined as in Equation (1):

$$m = \frac{1}{2} \int_V r \times j dv \quad (1)$$

This equation means that the circulated current around the closed conductive coil will cause a magnetic dipole. The SRR will be considered equivalent to the LC circuit. Such an equivalent LC circuit maximizes the electromagnetic responses under the external time-varying magnetic field H-field, normal to the plane of the SRRs as resonances occur. It is observed that there is a pair of capacitances in half of the ring, functioning as a series connection of two capacitances, as show in Figure 2. If we ignore the Ohmic loss, there will be a resonator that has a resonance frequency proportional to  $1/(LC)^{1/2}$ . The strength of the artificial magnetic dipole will be enhanced several times in relation to LC resonance at a specific frequency. Furthermore, we can calculate the effective permeability at different frequencies, as in Equation (2) [29]:

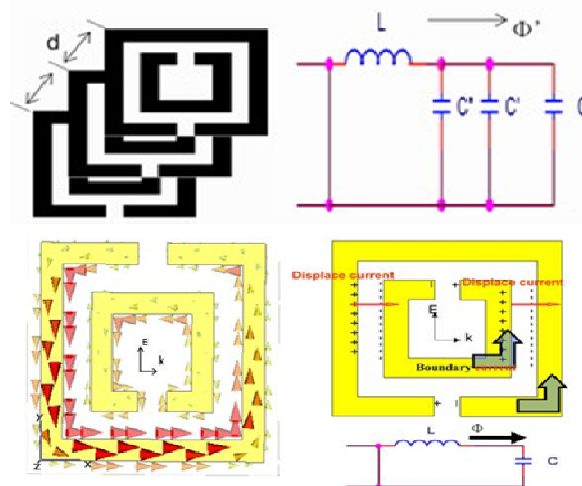
$$\mu_{eff}(\omega) = 1 - \frac{F\omega^2}{\omega^2 - \omega_0^2 + i\omega\Gamma} \quad (2)$$

In an experiment setting, the split-ring piling—as in Figure 2 are regarded as magnetic response enhancement. One can assume that the voltage distribution to the capacitance is using a parallel connection in an equivalence circuit, as shown on the right side of Figure 2. This set-up will increase the total capacitance value as  $C_{total} = C_{gap} + C_{parallel}$ . In references [30–39], many researchers have systematically investigated the properties of SRR, such as the size and the shape of the SRRs, the size of the unit cell, dielectric properties of the substrate, complementary structures of SRR, and the orientation relative to incident waves in the microwave region.

The development of the field of SRR, or magnetic metamaterials, has taken a new turn since nano-engineering and micro-system techniques became more complex. Indeed, the resonance frequency of SRR structures is determined by their sizes rather than their constituents, indicating that

one can further construct magnetism from microwaves to higher-frequency regions by simply miniaturizing the dimensions of constituent elements. By using micro-fabrication processes, researchers created artificial magnetism for 1 THz [40]; moreover, through nano-fabrication processes, researchers achieved magnetic resonance frequency at 100 THz [41]. Notice that a single-ring SRR with one cut also yields a significant magnetic response. However, the saturated magnetic resonance frequency occurs at 373 THz in conventional SRR design, restricting the artificial magnetic responses to the optical range [42]. As a consequence, research [43,44] has reported that modified SRRs introducing extra multi-cuts into the metallic rings can exhibit higher LC resonance frequencies and can even help boost the saturation frequency up to 550 THz [43], significantly easing the fabrication burden of high-frequency applications based on the SRR structures.

**Figure 2.** When split rings resonators are piled in a pure H-field, the induced current will not follow the flow of the original circuit. In particular, the layers are very close to one another because the capacitances of different layers are similar to the capacitance of the original layer; hence, the equivalence circuit will correspond to a parallel connection.



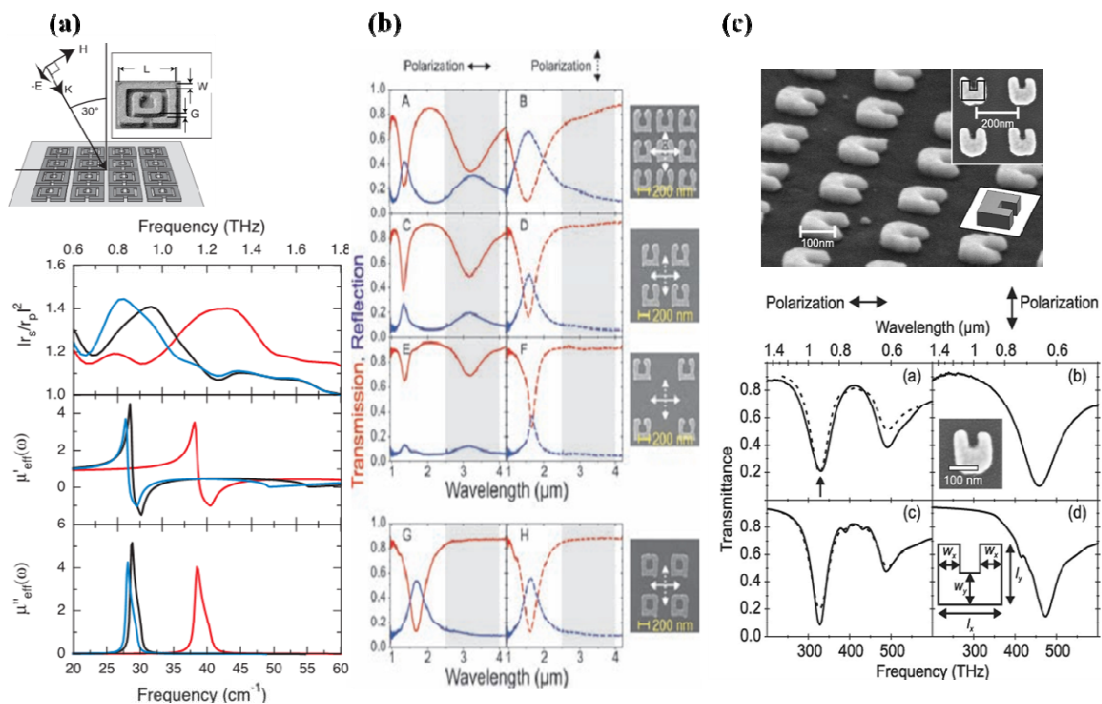
Apart from the issue of the SRR saturation frequencies, another crucial and problematic issue for applications of high-frequency magnetism relates to the polarization of incident light. Surprisingly, there is a transmission dip at the magnetic response frequency of the SRR, which means that an external electric field can also excite SRR [38,39]. More specifically, as the electric polarization is parallel to the split side of the SRRs, the magnetic resonance is excited through the induced current circulating within the SRRs, which is called electric excitation of magnetic resonance (or the EEMR effect) [38]. Such an electric excitation under normal incidence allows for a more attainable method to realize high-frequency responses toward nano-photonics applications.

The concept of a gap-capacitive LC circuit model makes it possible to estimate the fundamental resonances of the SRRs; nevertheless, additional multiple plasmonic resonances of SRRs [35,44–47] were also numerically and experimentally observed recently, an outcome that cannot be interpreted by reference to the gap-capacitive LC circuit model and that still requires a clear explanation. As a consequence, a general model of standing-wave plasmonic resonances reveals the possibility of interpreting SRRs' multiple responses under orthogonal electric excitations. The standing-wave plasmonic resonance (SWPR) model corresponds to the following Equation [47]:

$$L = \frac{m (\lambda_m + \lambda_0)}{2 n_{eff}} \quad (3)$$

where  $L$  denotes the total length of SRR,  $\lambda_m$  the resonance wavelength,  $m$  the resonance mode,  $n_{eff}$  the effective refractive index of the dielectric environment, and  $\lambda_0$  depends only on the geometric structure. Notice that the multiple reflectance peaks are denoted as two sets of resonance modes:  $1_{\parallel}$ ,  $3_{\parallel}$ ,  $5_{\parallel}$ ,  $7_{\parallel}$  and  $2_{\perp}$ ,  $4_{\perp}$ ,  $6_{\perp}$ ,  $8_{\perp}$  corresponding to two orthogonal E-filed polarization directions ( $E_{\parallel}$  and  $E_{\perp}$ ) in Figure 4(a), respectively. Then, one can plot the resonance wavelengths ( $\lambda_m$ ) versus the reciprocal of the resonance mode ( $1/m$ ) among different-sized SRRs. As shown in Figure 4(b), all curves show a clear linear relationship and among them, the longer SRR displays a greater slope that is consistent with Equation (3). In general, the model of standing-wave plasmonic resonances, indeed, explicitly provides the universal expression for the multiple resonances in SRRs and additionally allows us to accurately estimate the wavelengths, modes, and responses of those plasmonic resonances.

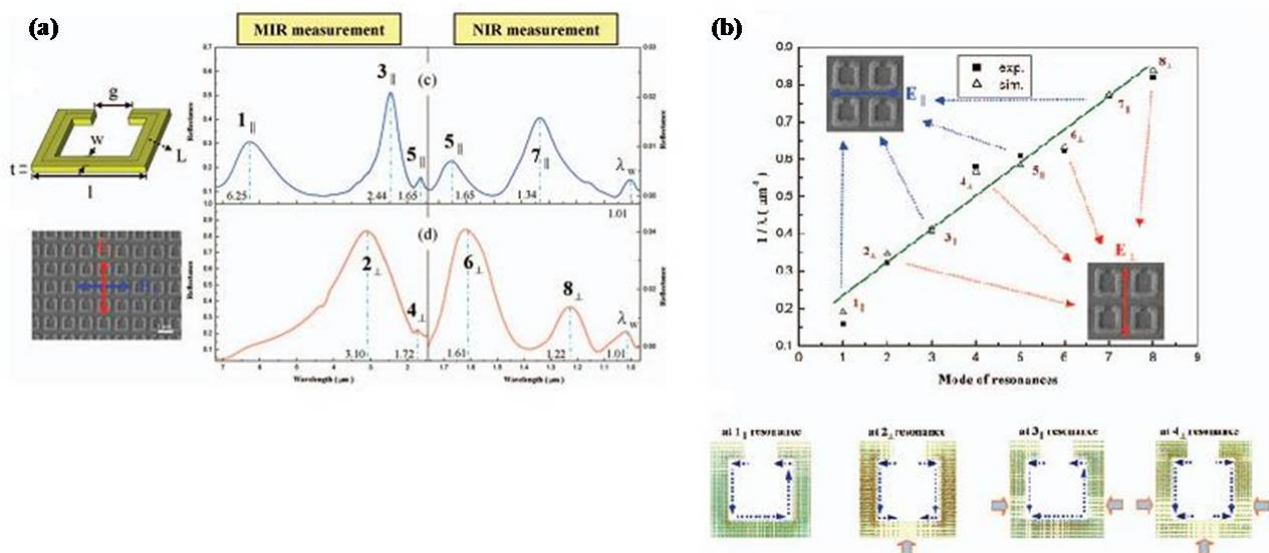
**Figure 3.** Different sized split ring resonators work at different wavelengths. (a) By using micro-fabrication process, the artificial magnetism can be realized at 1 THz [40]; (b) By using electron beam writing process and normal incidence into SRR planes, the magnetic response can be blue-shifted to 100 THz [41]; (c) By shrinking the dimension of the SRR size, the resonance response can be shifted to 373 THz in conventional SRR design [42].



Recently, more and more research interest has focused on tunable SRR devices and SRR-based biosensors for label-free sensing of chemical and biochemical materials. Intense research interest has focused on active control of the electromagnetic responses for functional devices such as modulators, filters, polarizers, and switches. Tunable resonance can be achieved through optical or voltage control of the capacitive response of SRRs [13,48–51]. Another approach is to fabricate anisotropic SRR structures that are reconfigurable in response to an external stimulus such as a thermal effect [52]. Label-free, coupler-free, and refractive-index SRR-based biosensors have undergone significant

development due to the capacitance of SRR structures' high sensitivity relative to external environments [53–55]. We expect that, in the near future, the findings of such successful demonstrations, by using a given SRR structure, can be readily extended to applications in our lives.

**Figure 4.** (a) The experiment measurement of the SRRs with related structural parameters. Two orthogonal polarized excitations ( $E_{\perp}$  and  $E_{\parallel}$ ) are indicated in blue and red and their corresponding spectra scanning from mid-infrared to near-infrared regions are shown in the figure, respectively; (b) In the upper part of the figure, the reciprocal values of multiple resonance wavelengths from the experiment (solid squares) and the simulation (hollow triangles) are plotted vs. the mode numbers, showing a clear linear relationship (green line). The lower part of the figure presents simulated distributions of the induced currents for the first four resonances, respectively. The arrows denote the directions of the induced currents, and then several distinct nodes corresponding to different resonant states [47].



## 2.2. Sandwich Structures (Fishnet Structures)

In general, LHM is an artificial material and consists of both a magnetic dipole providing a negative magnetic permeability  $\mu < 0$  and a plasmonic wire array yielding a negative electric permittivity  $\epsilon < 0$  [56–58]. To obtain negative magnetic permeability for these structures, the basic idea is to create a sufficiently strong magnetic resonance by first creating induced currents in two parallel metal strips excited by an external magnetic field (H-field). The pairs of metal strips are closely related to pairs of rods, for which there is an optical diamagnetic response, and Shalaev *et al.* reveal that a pair of strips can replace the previous resonators for the magnetic resonance, as shown in Figure 5 [59,60].

After combining the strip pairs with continuous metallic wires functioning as a diluted metal below the effective plasma frequency (as shown in Figure 6), both the negative magnetic permeability from parallel strips and the negative electric permittivity from continuous wires lead to a negative index of refraction. The new LHM design is called “fishnet structure metamaterial”.

Theoretical modeling of the metal-dielectric-metal strip metamaterials is performed by using effective inductor–capacitor circuits (LC circuit). An LC circuit model for the fishnet structure was

given in [19]. The model predicts the dependence of magnetic resonance frequency on the structure's parameters by way of the formula:

$$f_m = \sqrt{\frac{1}{l_1^2} + \frac{w_2}{l_1 l_2 a_x}} \quad (4)$$

Where  $l_2 = (a_y - l_1/2)$ ,  $l_1$  is the cut-wire length,  $w_2$  the wire width, and  $a_x$  and  $a_y$  are the periodicity in the  $x$  and  $y$  directions, see Figure 6.

**Figure 5.** (a) Regarding plate pairs as magnetic atoms for optical metamaterials, the schematic is the array of parallel-strip pairs, and the magnetic field of incident light was polarized as perpendicular to the strips. The blue vector refers to the induced current on the metallic strips; (b) Field-emission scanning electron microscope images for parallel-strip pairs [59].

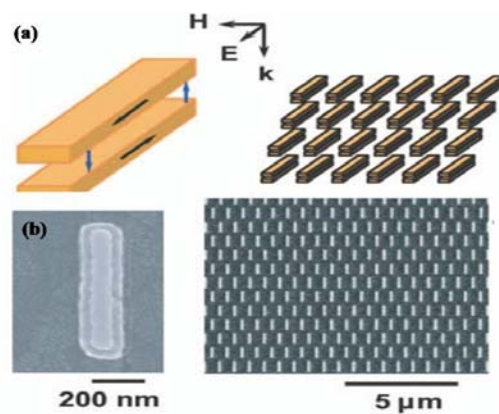
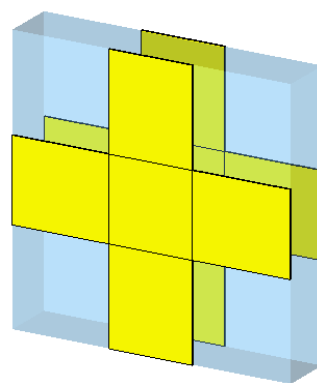


**Figure 6.** The geometry and parameters of one unit cell of the fishnet metamaterial. The electromagnetic wave propagates along the  $z$  direction, and the electric and magnetic fields are orthogonal.



In various types of metamaterials, the metal-dielectric-metal fishnet structure is at the heart of the first demonstrations of the optical negative index. The major reasons for this stem from easing its fabrication and excitation—for example, the fishnet structure can be fabricated within one lithographic process to harvest the negative refractive index directly rather than multiple ones to integrate plasmonic wires (for  $-\epsilon$ ) and split-ring resonators (for  $-\mu$ ); besides, the fishnet structure are operated under normal excitation and in fact these two points are particular critical for high-frequency application. In addition, The fishnet structure is polarization-independent and also a better design to

boost the performance of figure of merit (FOM), defined by the ratio between the real ( $n'$ ) and imaginary parts ( $n''$ ) of refractive indices ( $n'/n''$ ), which is crucial in the optical and the visible regime because the performance of metamaterials are dominated by this ratio. By means of fishnet structures, recently Dolling *et al.* [61,62] reached FOM = 3 at a wavelength of 1400 nm, and further used silver to evolve the first negative-index metamaterials at the visible spectrum of 780 nm wavelength [63]. More recently, Zhang's group successfully stacked up multiple fishnet functional layers along the wave propagation direction, so that the stacked fishnet metamaterials behave as "bulk" optical NRIM with a very high FOM of 3.5 [64]. The bulk optical metamaterials present the possibility of 3D optical effects and applications associated with NRIM, such as zero-index materials, superlenses, optical tunneling devices, compact resonators, and highly directional sources.

### 2.3. High-Permittivity Dielectric Composites

Many famous artificial magnetic metamaterials are based on metallic structures. Researchers have made a considerable effort to scale down metallic structures toward high-frequency applications in the infrared [40,41,65] and even the optical regions [66,67]. Unfortunately, present metallic resonators suffer from significant conduction loss and strong anisotropic properties that tarnish the performance, so recently, O'Brien and Pendry proposed a "high permittivity"-based (e.g., BST, LiTaO<sub>3</sub>, SiC) dielectric resonator array that is characterized by negative effective permeability for constructing artificial magnetic dipoles, and the proposal reflects the array's advantages in terms of both low loss and symmetric design [68,69]. Rather than use the LC-resonance of the conducting split rings to attain negative permeability as an average quantity, the mechanism proposed involves the well-known "Mie resonance" in dielectric particles [70].

From references [71,72], one could start by considering a single isolated dielectric sphere with radius  $r_o$  and relative permittivity  $\epsilon_s = n_s^2$ , embedded in a host with relative permittivity  $\epsilon_h = n_h^2$ . For an incident plane wave, the generalized dipole coefficients reduce to those in Mie theory, where

$$a_n = \frac{n_s \psi_n(n_s x) \psi_n'(n_h x) - n_h \psi_n(n_h x) \psi_n'(n_s x)}{n_s \psi_n(n_s x) \xi_n'(n_h x) - n_h \xi_n(n_h x) \psi_n'(n_s x)} \quad (5)$$

$$b_n = \frac{n_h \psi_n(n_s x) \psi_n'(n_h x) - n_s \psi_n(n_h x) \psi_n'(n_s x)}{n_h \psi_n(n_s x) \xi_n'(n_h x) - n_s \xi_n(n_h x) \psi_n'(n_s x)} \quad (6)$$

Here,  $x = k_o r_o$ , and  $\psi_n(x)$  and  $\xi_n(x)$  are the Riccati-Bessel function, and the primes indicate differentiation with respect to the argument. With regards to effective permeability and permittivity, only the  $b_1$  coefficient representing the strength of the magnetic dipole response and the  $a_1$  coefficient representing the strength of the electric dipole response should be of concern. The dipole term contributes mainly to the scattered magnetic field in the far field (see the following equation):

$$H_{sca} = -\frac{3i}{2} H_o b_1 \frac{e^{i k_o r}}{k_o r} \bar{r} \times (\bar{r} \times \bar{y}) \quad (7)$$

If the wavelength of an incident wave is much larger than the size of the sphere, one could use a radiating magnetic dipole moment  $m$  to replace the sphere. Therefore, the radiated field matches the standard far-field expression of dipole radiation [73]:

$$H_{dipole} = -\frac{k_o^3}{4\pi k_o r} e^{ik_o r} \bar{r} \times (\bar{r} \times \bar{m}) \quad (8)$$

We could get the equivalent magnetic dipole moment of a single dielectric sphere particle by equating the two equations above, and then there would be a relationship between the induced magnetic dipole moment and incident magnetic field, as in the equation

$$m = \alpha_m H_{inc} \quad (9)$$

where  $\alpha_m$  is the magnetic polarizability. The response of an ensemble of such magnetic dipoles can be dictated by effective permeability  $\mu_r^{eff}$ . The magnetic polarizability  $\alpha_m$  and effective permeability  $\mu_r^{eff}$  are connected by the Clausius-Mossotti equation [74],

$$\alpha_m = \frac{3}{N} \left( \frac{\mu_r^{eff} - 1}{\mu_r^{eff} + 2} \right) \quad (10)$$

$$f = \frac{4\pi N r_o^3}{3}$$

where  $f$  is the filling fraction of composites and  $N$  is the volume density of the dipoles. The effective permeability ( $\mu_r^{eff}$ ) and permittivity ( $\epsilon_r^{eff}$ ) are described by the following equation:

$$\mu_r^{eff} = \frac{k_o^3 + 4\pi i N b_1}{k_o^3 - 2\pi i N b_1} \quad (11)$$

$$\epsilon_r^{eff} = \frac{k_o^3 + 4\pi i N a_1}{k_o^3 - 2\pi i N a_1}$$

one can determine the effective electromagnetic parameters in the long-wavelength limit by following the above calculation.

In fact, arrays of dielectric rods in p-polarized light have been shown to possess an effective negative magnetic permeability [68,75]. Moreover, arrays of the dielectric rods in s-polarized light present both magnetic and electric dipole resonances, implying that NRIM with simultaneously negative permeability and permittivity could be realized by all dielectric resonators [76,77]. Actually, dielectric elements naturally only have a strong electric response, but from the viewpoint of metamaterials, artificial magnetic and electric resonances are introduced in the dielectric particles and are further enhanced by the Mie resonance [70] that is analog to LC resonance for SRRs [16]. The localized magnetic or electric resonance mode from the Mie resonance in an array of high-dielectric-constant particles could bring about macroscopic bulk magnetization or polarization in the medium, giving rise to either non-zero magnetic susceptibility or electric susceptibility on average [68]. Therefore, it is theoretically possible to construct the NRIM by properly combining the negative  $\mu_r$  and  $\epsilon_r$  from two series of dielectric resonators with different dielectric constants at the same frequency region [78]. An alternate approach is to integrate the negative  $\mu_r$  from periodically arranged dielectric particles as well as the negative  $\epsilon_r$  from plasmonic wires [79]. However, it is inconvenient to fabricate NRIM for practical devices with either of these approaches owing to the multiple-step fabrication process. Therefore, Vendik and Gashinova have theoretically investigated the possibility that the effective isotropic negative refractive index medium is realizable through the use of two

different dielectric sphere lattices embedded in a dielectric matrix [80], and in this regard, experimental verification has been completed recently [21,81]. The underlying physics is explicit since the magnetic fundamental resonance mode and electrical resonance mode can be overlapped by scaling the size and the lattice of the dielectric inclusions. However, it was found experimentally that the resonant response of the electric dipole was weakly pronounced, and that negative refraction behavior was remarkably suppressed. In order to enhance the electric dipole resonance, some researchers considered the symmetry of the bi-spherical arrangement of the particles corresponding to the body-centered cubic symmetry because of the increasing packing factor [82]. For practical realization, the concept of metamaterials based on cubic dielectric inclusions is preferable.

Isotropy is another advantage of using dielectric metamaterials. Q. Zhao *et al.* have been experimentally demonstrating isotropic negative permeability in three-dimensional dielectric composites [83] and have been using the thermal properties of ceramic materials to realize, experimentally, an actively modulated isotropic negative permeability [84]. The critical challenge for dielectric metamaterials is that there is no high permeability-based material in optical range so that, until now, researchers have given up on the electric and magnetic dipole activities of dielectric composites. However, the theory of using silicon-based ( $\epsilon = 12$ ) rod-type structures has been reported recently, thereby relaxing the metamaterials criterion with basic cell dimensions, which are significant with respect to wavelength [85]. Reference 85 shows a similar band structure calculated between “high permittivity”-based and “low permittivity”-based dielectric composites, and the behavior of finding negative refraction in silicon-based dielectric rod arrays is discussed. Such a moderate relative-permittivity value has the further advantage of significantly easing the fabrication limitations because the corresponding cell dimension of the dielectric resonators turns out to be greater than the wavelength of light. As a result, we expect that research in the near future, by using both dielectric resonators with a moderate relative-permittivity value and such relative applications as all-dielectric invisibility cloaks [86], can readily extend the aforementioned demonstrations to optics.

### 3. Extended Applications

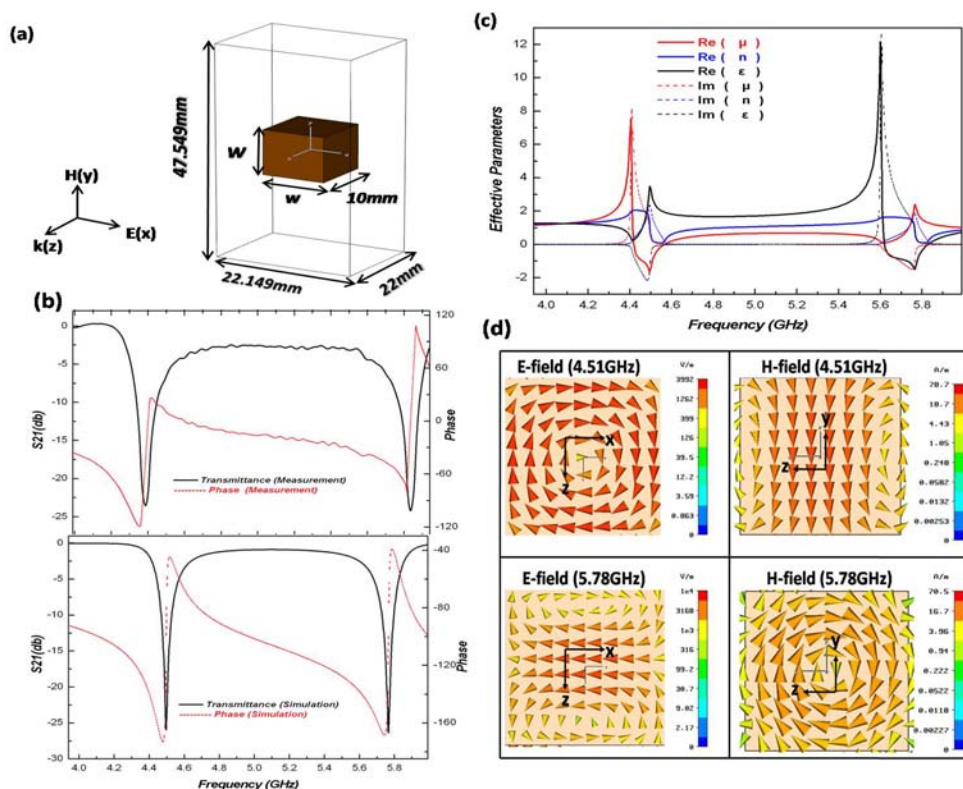
There has been intense research on metamaterials in this decade, and recently there has been an increasing focus on practical applications for metamaterials. In this section, we will address fascinating investigations and practical applications of artificial electromagnetic metamaterials that are serving to overcome the intrinsic limitations of naturally existing materials. This section of the paper will address magnetic walls, magnetic surface plasmon resonance, invisibility cloaking, artificial electromagnetically induced transparency, and the slow light effect.

#### 3.1. Magnetic Walls

In optics, spectral selectivity components (such as beam splitters, filters, and mirrors) traditionally use interference of light in dielectric multilayers or photonic crystal. However, the thickness of these devices is comparable to wavelength. A thin, essentially subwavelength layer that directly concerns neither interference nor diffraction is an opportunity to achieve spectral selectivity. A planar metamaterial with metallic fishscale-pattern layers and with metallic back-plates satisfies the requisition [87,88]. The new type of planar fishscale metamaterial possesses some peculiar properties,

such as high transparency, broad band reflectors, and reflected waves without phase change. The last property is extraordinary, insofar as conventional metals and dielectric surfaces reverse the electric field phase. Indeed  $(n - 1)E_{\text{reflected}} = -(n + 1)E_{\text{incident}}$ , and the result means that fishscale metamaterial has a zero refractive index; this phenomenon, when manifested, is called a “magnetic wall”. The unusual amplification properties herein can function to improve photodetectors. The nanofabrication techniques may well lead to the use of the fish-scale structures in the optical part of the spectrum.

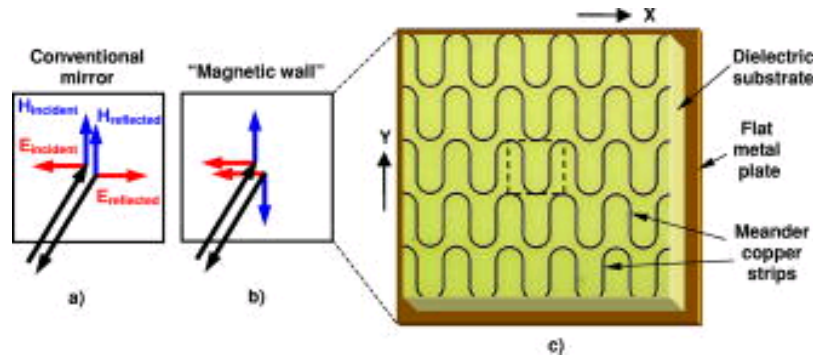
**Figure 7.** (a) Schematics of the unit cell of dielectric resonators in simulation ( $\text{ZrO}_2$ ;  $\epsilon_r = 33$ ;  $w = 6.5\text{--}10\text{ mm}$ , every  $0.5\text{ mm}$  in the space); (b) The measurement and simulation results (transmittance and phase) of the  $\text{ZrO}_2$  cubes being  $10 \times 10 \times 10\text{ mm}^3$  in size. The two sets of results are in good agreement, indicating that there were magnetic and electric resonances at  $4.51$  and  $5.78\text{ GHz}$ , respectively; (c) Effective material parameters (permeability, permittivity, and refractive index) of  $\text{ZrO}_2$  cube arrays ( $10\text{ mm}$  cubed) calculated by an inversion method, showing negative permeability and negative permittivity at two resonant states; (d) Electric-field distributions (left part) and magnetic-field distributions (right part) at a magnetic resonance frequency ( $4.51\text{ GHz}$ ; upper part) and those at an electric resonance frequency ( $5.78\text{ GHz}$ ; lower part). At  $4.51\text{ GHz}$  a circular displacement current ( $J_d = \epsilon_r \epsilon_0 dE/dt$ ) is excited by a time-varying magnetic field in the designed dielectric resonators, as shown in the upper panel. Such a  $J_d$  plays a role similar to that of the conduction current ( $J_c$ ) in metal-based metamaterials, then resulting in a significant magnetic dipole at resonance. Notice a magnetic dipole oriented along the  $y$ -direction at  $4.51\text{ GHz}$ , and an electric dipole oriented along the  $x$ -direction at  $5.78\text{ GHz}$ . [21]



### 3.2. Magnetic Surface Plasmon Resonance

Electric surface plasmon resonance (SPR) demonstrated by an electron energy-loss experiment [89] in 1960 exists between the two medium with opposed sign of permittivity. In addition, the electric SPR can be excited by visible light with two methods, grating coupler and ATR coupler. With the help of those couplers, the electric surface plasmon resonance becomes a powerful tool to detect the chemical and physical phenomena for optical frequency band. As for magnetic SPR, the experiments [90–94] also were demonstrated at microwave regions in 1981. However, due to the weakness of magnetic response for optical frequencies, there are no experimental results so far.

**Figure 8.** Reflection field schematic of a conventional mirror (a) and a magnetic wall mirror (b). Figure (c) shows the magnetic wall mirror consisting of metallic fish-scale pattern on a thickness dielectric substrate backed with a flat metal mirror [88].



According to the Maxwell's equations, one could simply replace the permittivity by permeability for dispersion equation for isotropic, homogeneous, and linear media.

$$\text{Electric SPR } k_x = \sqrt{\frac{\varepsilon_1 \varepsilon_2}{\varepsilon_1 + \varepsilon_2}} \quad (\text{for pure dielectrics}) \quad (12)$$

$$\text{Magnetic SPR } k_x = \sqrt{\frac{\mu_1 \mu_2}{\mu_1 + \mu_2}} \quad (\text{for pure magnetic medium}) \quad (13)$$

In 2005, magnetic metamaterials [95] (split-ring resonator) showed that magnetic SPR can be created by artificial method which means we may tune the frequency of magnetic SPR to any desired frequency. This result would open up the possibility of magnetic SPR at optical frequency band.

### 3.3. Invisibility Cloaking

Transformation optics, based on the non-relativistic coordination invariance of Maxwell's equations, allows metamaterials to achieve exciting electromagnetic properties with practical designs. The most famous application developed is very likely the circular cloaking device, which was mathematically proposed by Pendry *et al.* [96] and experimentally demonstrated by Smith's groups [12,97,98] in 2006: the entire effort rested on extruding EM waves within a certain region through carefully designed constitutive parameters.

Two main steps are included in the transformation design method. Firstly, a particular coordinate transformation between physical space  $\mathbf{x}$  and transformed space  $\mathbf{x}'$  is constructed according to the

designed property (free space properties in transformed space for invisibility). Secondly, the constitutive parameter tensors of the transformation medium that realizes the coordinate transformation can be obtained by using the following equations

$$\begin{aligned}\varepsilon'(\mathbf{x}') &= \frac{\hat{\varepsilon} \varepsilon(\mathbf{x}) \hat{\varepsilon}^T}{\det \hat{\varepsilon}} \\ \mu'(\mathbf{x}') &= \frac{\hat{\mu} \mu(\mathbf{x}) \hat{\mu}^T}{\det \hat{\mu}}\end{aligned}\quad (14)$$

And  $\hat{\varepsilon}$  is the well-known Jacobian transformation tensor with components  $\partial x_i / \partial x'_j$ . The transformed media are generally anisotropic and spatially dispersive.

Recently, another novel cloaking device based on transformation optics has been proposed by C.T. Chan [99]. Such a cloaking device, the so-called external cloak, can make an object invisible external to the cloak. The idea can be understood as follows: a complementary medium, when designed according to transformation optics, optically cancels the scattering wave with the cloaked object. Then the optical path of free space is restored in the restoration medium. Furthermore, an illusion device optically transforming an object to another has been proposed on the basis of optical cancellation and restoration [100]. As a consequence, the external cloaking device creates the illusion of free space. However, the requirement of anisotropies, spatial dispersion, and the negative refraction index for the complementary medium constitutes a considerable challenge to realizing the external cloaking device.

### 3.4. Artificial Electromagnetically Induced Transparency

In quantum mechanics theory, the coherent coupling among three energy levels leads to quantum interference known as the electromagnetically induced transparency (EIT) effect, which possesses the potential to slow down light pulses dramatically or even to stop light pulses owing to the highly dispersive relationship between wave vector and frequency at transparent window [101]. However, for a conventional quantum EIT effect, the media in use are often ultra-cold or ultra-hot gases, which limit the application of EIT effect, although solid-state media are believed to exhibit the EIT effect in theory [102].

Based on the same idea as conventional electromagnetically induced transparency, many research works are focusing on metamaterials possessing properties analogous to the EIT effect. Xiang Zhang's group has demonstrated that when coupling the plasmonic superradiant (bright) mode and the plasmonic subradiant (dark) mode together, Zhang, X's group would mimic the system comprising three energy levels for the conventional EIT effect by using two metamaterial atoms, and they claims that metamaterials possessing properties analogous to the EIT effect have advantages such as room-temperature operation, wide bandwidth, and, more importantly, ready integration with a nano-plasmonic circuit [103].

To further reduce losses of metamaterial-analogue EIT effect, researchers have suggested the introduction of stacked optical asymmetric metamaterials. As shown in ref [104], a dipole antenna of broad linewidth is coupled with a quadrupole one of narrow linewidth determined by non-radiative Drude damping. Here, Liu, N. *et al* claims that this coupled system dramatically reduces the losses relative to the EIT system, due to nearly complete suppression of radiative coupling. Moreover, the loss is, in fact, even smaller than the losses from intrinsic Drude damping, which represents highly

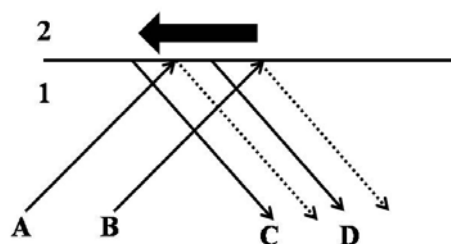
suppression of non-radiative damping. Such a metamaterial-analogue EIT effect not only reduces losses for the optical devices but also creates a solid-state unit to be integrated into optical circuits. Finally, the system has been recently applied to high-sensitivity biosensors because of the substantial dispersion relationship [105].

### 3.5. Slow-Light Effect by NRM

Regarding positive-refractive-index materials, momentum mismatch can create a situation where radiative waves cannot couple directly to the surface polaritons at the interfaces of the slab [106]. Thus, researchers excite surface plasmon polariton at interface of positive permeability and negative permittivity. Furthermore, researchers construct a dielectric-metal-dielectric structure as a sandwiched slab waveguide to generate two SPPs at different interfaces between metal and dielectric. Once the two SPPs couple to each other, the calculated effective group velocity would achieve zero in a certain critical thickness, *i.e.*, they can slow or stop light, indicating that they can store light within a waveguide [106].

Recently, the topic of slow light has garnered considerable attention because slow light is potentially applicable to optical switching and to storage devices like optical hard disks [14,106–110]. But in SPP mode, left-handed slab waveguides are very sensitive to surface roughness and operate in multiple modes [108]. Therefore, researchers have made the core material a left-handed material to construct a left-handed sandwiched slab waveguide, making possible a single oscillatory mode that propagates within the core material and that can be stopped at a critical thickness because of a negative Goos-Hanchen effect (as shown in Figure 9) [111–113]. Furthermore, research has demonstrated that a multi frequency waveguide can store ‘rainbows’ in a core material possessing a negative refractive index [14,114].

**Figure 9.** A schematic representation of the Goos-Hanchen shift  $d$ . AB is the incident beam and CD the reflected beam. Medium 2 is negatively refractive with energy flow to the left [113].



## 4. Conclusions

In this paper, we have summarized the recent branch of research focusing on artificial magnetic metamaterials. We first introduced some artificial metallic structures that enrich magnetic responses in ways that are foreign to natural materials. Because there is high Ohmic loss in metallic structures in the optical region, researchers have posited that “high permittivity”-based dielectric composite arrays enrich the symmetry of the metamaterials field. In addition, we have introduced some applications for metamaterials and outlined some new directions. Magnetic walls, magnetic surface plasma resonance,

invisible cloaking, an artificial electromagnetically induced transparency effect, and a slowing-light effect are included in this review. A newly designed NRIM can be readily implemented in various applications like flat-focusing lenses, band-pass and notch filters, antennas, invisible cloaking, and various electromagnetic devices.

### Acknowledgements

The authors would like to gratefully acknowledge the financial support from National Science Council (NSC98-2112-M-007-002MY3, NSC99-2120-M-002-012, and NSC99-2120-M-010-001), and from the Ministry of Education (“Aim for the Top University Plan” for National Tsing Hua University).

### References

1. Pimenov, A.; Loidl, A.; Gehrke, K.; Moshnyaga, V.; Samwer, K. Negative refraction observed in a metallic ferromagnet in the gigahertz frequency range. *Phys. Rev. Lett.* **2007**, *98*, 197401.
2. Rachford, F.J.; Armstead, D.; Harris, V.; Vittoria, C. Simulations of ferrite-dielectric-wire composite negative index materials. *Phys. Rev. Lett.* **2007**, *99*, 057202.
3. Shelby, R.A.; Smith, D.R.; Schultz, S. Experimental verification of a negative index of refraction. *Science* **2001**, *292*, 77–79.
4. Pendry, J.B. A chiral route to negative refraction. *Science* **2004**, *306*, 1353–1355.
5. Seddon, N.; Bearpark, T. Observation of the inverse Doppler effect. *Science* **2003**, *302*, 1537–1540.
6. Lu, J.; Grzegorzczak, T.; Zhang, Y.; Pacheco, J., Jr.; Wu, B.I.; Kong, J.; Chen, M. Cerenkov radiation in materials with negative permittivity and permeability. *Opt. Express* **2003**, *11*, 723–724.
7. Taubner, T.; Korobkin, D.; Urzhumov, Y.; Shvets, G.; Hillenbrand, R. Near-field microscopy through a SiC superlens. *Science* **2006**, *313*, 1595.
8. Merlin, R. Analytical solution of the almost-perfect lens problem. *Appl. Phys. Lett.* **2004**, *84*, 1290–1292.
9. Grbic, A.; Eleftheriades, G.V. Overcoming the diffraction limit with a planar left-handed transmission-line lens. *Phys. Rev. Lett.* **2004**, *92*, 117403.
10. Narimanov, E.E.; Shalaev, V.M. Optics: Beyond diffraction. *Nature* **2007**, *447*, 266–267.
11. Pendry, J.B. Negative refraction makes a perfect lens. *Phys. Rev. Lett.* **2000**, *85*, 3966–3969.
12. Schurig, D.; Mock, J.J.; Justice, B.J.; Cummer, S.A.; Pendry, J.B.; Starr, A.F.; Smith, D.R. Metamaterial electromagnetic cloak at microwave frequencies. *Science* **2006**, *314*, 977–980.
13. Chen, H.T.; Padilla, W.J.; Zide, J.M.O.; Gossard, A.C.; Taylor, A.J.; Averitt, R.D. Active terahertz metamaterials devices. *Nature* **2006**, *444*, 597–600.
14. Tsakmakidis, K.L.; Boardman, A.D.; Hess, O. Trapped rainbow storage of light in metamaterials. *Nature* **2007**, *450*, 397–401.
15. Veselago, G. The electrodynamics of substances with simultaneously negative values of  $\epsilon$  and  $\mu$ . *Sov. Phys. Usp.* **1968**, *10*, 509–514.
16. Pendry, J.B.; Holden, A.J.; Robbins, D.J.; Stewart, W.J. Magnetism from conductors and enhanced nonlinear phenomena. *IEEE Trans. Microw. Theory Tech.* **1999**, *47*, 2075–2084.
17. Reynet, O.; Acher, O. Voltage controlled metamaterials. *Appl. Phys. Lett.* **2004**, *84*, 1198–2000.

18. Wiltshire, M.C.K.; Pendry, J.B.; Young, I.R.; Larkman, D.J.; Gilderdale D.J.; Hajnal, J.V. Microstructured magnetic materials for RF flux guides in magnetic resonance imaging. *Science* **2001**, *291*, 849–851.
19. Zhang, S.; Fan, W.; Panoiu, N.C.; Malloy, K.J.; Osgood, R.M.; Brueck, S.R. Experimental demonstration of near-infrared negative-index metamaterials. *Phys. Rev. Lett.* **2005**, *95*, 137404.
20. Alici, K.B.; Ozbay, E. A planar metamaterial: Polarization independent fishnet structure. *Photonics Nanostruct.* **2008**, *6*, 102–107.
21. Lai, Y.J.; Chen, C.K.; Yen, T.J. Creating negative refractive identity via single-dielectric resonators. *Opt. Express* **2009**, *17*, 12960–12970.
22. Lomakin, V.; Fainman, Y.; Urzhumov, Y.; Shvets, G. Doubly negative metamaterials in the near infrared and visible regimes based on thin film nanocomposites. *Opt. Express* **2006**, *14*, 11164–11177.
23. Chiang, Y.J.; Yen, T.J. A highly symmetric two-handed metamaterial spontaneously matching the wave impedance. *Opt. Express* **2008**, *16*, 12764–12770.
24. Smith, D.R.; Schultz, S.; Markoš, P.; Soukoulis, C.M. Determination of effective permittivity and permeability of metamaterials from reflection and transmission coefficients. *Phys. Rev. B* **2002**, *65*, 195104.
25. Chen, X.; Grzegorzczak, T.M.; Wu, B.I.; Pacheco, J., Jr.; Kong, J.A. Robust method to retrieve the constitutive effective parameters of metamaterials. *Phys. Rev. E* **2004**, *70*, 016608.
26. Smith, D.R.; Vier, D.C.; Koschny, T.; Soukoulis, C.M. Electromagnetic parameter retrieval from inhomogeneous metamaterials. *Phys. Rev. E* **2005**, *71*, 036617.
27. Dolling, G.; Enkrich, C.; Wegener, M.; Zhou, J.F.; Soukoulis, C.M.; Linden, S. Cut-wire pairs and plate pairs as magnetic atoms for optical metamaterials. *Opt. Lett.* **2006**, *30*, 3198–3200.
28. Gay-Balmaz, P.; Martin, O.J.F. Efficient isotropic magnetic resonators. *Appl. Phys. Lett.* **2002**, *81*, 939–941.
29. Mills, D.L.; Burstein, E. Polaritons: The electromagnetic modes of media. *Rep. Prog. Phys.* **1974**, *37*, 817–926.
30. Smith, D.R.; Padilla, W.J.; Vier, D.C.; Nemat-Nasser, S.C.; Schultz, S. Composite medium with simultaneously negative permeability and permittivity. *Phys. Rev. Lett.* **2000**, *84*, 4184.
31. Weiland, T.; Schuhmann, R. *Ab initio* numerical simulation of left-handed metamaterials: Comparison of calculations and experiments. *J. Appl. Phys.* **2001**, *90*, 5419.
32. Shelby, R.A.; Smith, D.; Nemat-Nasser, S.; Schultz, S. Microwave transmission through a two-dimensional, isotropic, left-handed metamaterials. *Appl. Phys. Lett.* **2001**, *78*, 489–491.
33. Marqués, R.; Martel, J.; Mesa, F.; Medina, F. A new 2D isotropic left-handed metamaterial design: theory and experiment. *Microw. Opt. Technol. Lett.* **2002**, *36*, 405.
34. Markoš, P.; Soukoulis, C.M. Numerical studies of left-handed materials and arrays of split ring resonators. *Phys. Rev. E* **2002**, *65*, 036622.
35. Rockstuhl, C.; Zentgraf, T.; Guo, H.; Liu, N.; Etrich, C.; Loa, I.; Syassen, K.; Kuhl, J.; Lederer, F.; Giessen, H. Resonances of split-ring resonator metamaterials in the near infrared. *Appl. Phys. B* **2006**, *84*, 219–227.
36. Falcone, F.; Lopetegui, T.; Laso, M.A.; Baena, J.D.; Bonache, J.; Beruete, M.; Marqués, R.; Martín, F.; Sorolla, M. Babinet principle applied to the design of metasurfaces and metamaterials. *Phys. Rev. Lett.* **2004**, *93*, 197401.

37. Marqués, R.; Medina, F.; Rafii-El-Idrissi, R. Role of bianisotropy in negative permeability and left-handed metamaterials. *Phys. Rev. B* **2002**, *65*, 144440.
38. Katsarakis, N.; Koschny, T.; Kafesaki, M. Electric coupling to the magnetic resonance of split ring resonators. *Appl. Phys. Lett.* **2004**, *84*, 2943–2945.
39. Kafesaki, M.; Koschny, T.; Penciu, R.S.; Gundogdu, T.F.; Economou, E.N.; Soukoulis, C.M. Left-handed metamaterials: detailed numerical studies of the transmission properties. *J. Opt. A: Pure Appl. Opt.* **2005**, *7*, S12–S22.
40. Yen, T.J.; Padilla, W.J.; Fang, N.; Vier, D.C.; Smith, D.R.; Pendry, J.B.; Basov, D.N.; Zhang, X. Terahertz magnetic response from artificial materials. *Science* **2004**, *303*, 1494–1496.
41. Linden, S.; Enkrich, C.; Wegener, M.; Zhou, J.; Koschny, T.; Soukoulis, C.M. Magnetic response of metamaterials at 100 terahertz. *Science* **2004**, *306*, 1351–1353.
42. Klein, M.W.; Enkrich, C.; Wegener, M.; Soukoulis, C.M.; Linden, S. Single-slit split-ring resonators at optical frequencies: Limits of size scaling. *Opt. Lett.* **2006**, *31*, 1259–1261.
43. Zhou, J.; Koschny, T.; Kafesaki, M.; Economou, E.N.; Pendry, J.B.; Soukoulis, C.M. Saturation of the magnetic response of split-ring resonators at optical frequencies. *Phys. Rev. Lett.* **2005**, *95*, 223902.
44. Soukoulis, C.M. Magnetic response of split ring resonators at terahertz frequencies. *Phys. Status Solidi B* **2007**, *244*, 1181–1187.
45. Rockstuhl, C. On the reinterpretation of resonances in split-ring-resonators at normal incidence. *Opt. Express* **2006**, *14*, 8827–8836.
46. Sheridan, A.K.; Clark, A.W.; Glidle, A.; Cooper, J.M.; Cumming, D.R.S. Multiple plasmon resonances from gold nanostructures. *Appl. Phys. Lett.* **2007**, *90*, 143105.
47. Chen, C.Y.; Wu, S.C.; Yen, T.J. Experimental verification of standing-wave plasmonic resonances in split-ring resonators. *Appl. Phys. Lett.* **2008**, *93*, 034110.
48. Padilla, W.J.; Taylor, A.J.; Highstrete, C.; Lee, M.; Averitt, R.D. Dynamical electric and magnetic metamaterial response at terahertz frequencies. *Phys. Rev. Lett.* **2006**, *96*, 107401.
49. Chen, H.T.; O’Hara, J.F.; Azad, A.K.; Taylor, A.J.; Averitt, R.D.; Shrekenhamer, D.B.; Padilla, W.J. Experimental demonstration of frequency-agile terahertz metamaterials. *Nat. Photon.* **2008**, *2*, 295.
50. Degiron, A.; Mock, J.J.; Smith, D.R. Modulating and tuning the response of metamaterials at the unit cell level. *Opt. Express* **2007**, *15*, 1115–1127.
51. Shadrivov, I.V.; Morrison, S.K.; Kivshar, Y.S. Tunable split-ring resonators for nonlinear negative-index metamaterials. *Opt. Express* **2006**, *14*, 9344–9349.
52. Tao, H.; Strikwerda, A.C.; Fan, K.; Padilla, W.J.; Zhang, X.; Averitt, R.D. Reconfigurable terahertz metamaterials. *Phys. Rev. Lett.* **2009**, *103*, 147401.
53. Driscoll, T.; Andreev, G.O.; Basov, D.N.; Palit, S.; Cho, S.Y.; Jokerst, N.M.; Smith, D.R. Tuned permeability in terahertz split-ring resonators for devices and sensors. *Appl. Phys. Lett.* **2007**, *91*, 062511.
54. Debus, C.; Bolivar, P.H. Frequency selective surfaces for high sensitivity terahertz sensing. *Appl. Phys. Lett.* **2007**, *91*, 184102.
55. Lahiri, B.; Khokhar, A.; De La Rue, R.; McMeekin, S.G.; Johnson, N. Asymmetric split ring resonators for optical sensing of organic materials. *Opt. Express* **2009**, *17*, 1107–1115.

56. Smith, D.R.; Pendry, J.B.; Wiltshire, M.C.K. Metamaterials and negative refractive index. *Science* **2004**, *305*, 788.
57. Soukoulis, C.M.; Linden, S.; Wegener, M. Negative refractive index at optical wavelengths. *Science* **2007**, *315*, 47.
58. Liu, Y.; Zhang, X. Metamaterials: A new frontier of science and technology. *Chem. Soc. Rev.* **2011**, *40*, 2494–2507.
59. Shalaev, V.M.; Cai, W.; Chettiar, U.K.; Yuan, H.K.; Sarychev, A.K.; Drachev, V.P.; Kildishev, A.V. Negative index of refraction in optical metamaterials. *Opt. Lett.* **2005**, *30*, 3356–3358.
60. Cai, W.; Chettiar, U.K.; Yuan, H.K.; de Silva, V.C.; Kildishev, A.V.; Drachev, V.P.; Shalaev, V.M. Metamagnetics with rainbow colors. *Opt. Express* **2007**, *15*, 3333–3341.
61. Dolling, G.; Enkrich, C.; Wegener, M.; Soukoulis, C.M.; Linden, S. Low-loss negative-index metamaterial at telecommunication wavelengths. *Opt. Lett.* **2006**, *31*, 1800–1802.
62. Dolling, G.; Enkrich, C.; Wegener, M.; Soukoulis, C.M.; Linden, S. Simultaneous negative phase and group velocity of light in a metamaterial. *Science* **2006**, *312*, 892–894.
63. Dolling, G.; Enkrich, C.; Wegener, M.; Soukoulis, C.M.; Linden, S. Negative-index metamaterial at 780 nm wavelength. *Opt. Lett.* **2007**, *32*, 53–55.
64. Valentine, J.; Zhang, S.; Zentgraf, T.; Ulin-Avila, E.; Genov, D.A.; Bartal, G.; Zhang, X. Three-dimensional optical metamaterial with a negative refractive index. *Nature* **2008**, *455*, 376–379.
65. Zhang, S.; Fan, W.; Malloy, K.J.; Brueck, S.R.; Panoiu, N.C.; Osgood, R.M. Near-infrared double negative metamaterials. *Opt. Express* **2005**, *13*, 4922–4930.
66. Lezec, H.J.; Dionne, J.A.; Atwater, H.A. Negative refraction at visible frequencies. *Science* **2007**, *316*, 430–432.
67. Yao, J.; Liu, Z.; Liu, Y.; Wang, Y.; Sun, C.; Bartal, G.; Stacy, A.M.; Zhang, X. Optical negative refraction in bulk metamaterials of nanowires. *Science* **2008**, *321*, 930–930.
68. O'Brien, S.; Pendry, J.B. Photonic band-gap effects and magnetic activity in dielectric composites. *J. Phys. Condens. Matter.* **2002**, *14*, 4035–4044.
69. Merlin, R. Metamaterials and the Landau-Lifshitz permeability argument: Large permittivity begets high-frequency magnetism. *Proc. Natl. Acad. Sci. USA* **2009**, *106*, 1693–1698.
70. Mie, G. Beiträge zur Optik trüber Medien, speziell kolloidaler Metallösungen. *Ann. Phys.* **1908**, *25*, 377–445.
71. Wheeler, M.S.; Aitchison, J.S.; Mojahedi, M. Three-dimensional array of dielectric spheres with an isotropic negative permeability at infrared frequencies. *Phys. Rev. B* **2005**, *72*, 193103.
72. Shvets, G.; Urzhumov, Y.A. Engineering the electromagnetic properties of periodic nanostructures using electrostatic resonances. *Phys. Rev. Lett.* **2004**, *93*, 243902.
73. Jackson, J.D. *Classical Electrodynamics*, 3rd ed.; John Wiley and Sons Inc.: New York, NY, USA, 1999.
74. Kittel, C. *Introduction to Solid State Physics*, 7th ed.; John Wiley and Sons Inc.: New York, NY, USA, 1996.
75. Felbacq, D.; Bouchitté, G. Theory of mesoscopic magnetism in photonic crystals. *Phys. Rev. Lett.* **2005**, *94*, 183902.

76. Peng, L.; Ran, L.; Chen, H.; Zhang, H.; Kong, J.A.; Grzegorzcyk, T.M. Experimental observation of left-handed behavior in an array of standard dielectric resonators. *Phys. Rev. Lett.* **2007**, *98*, 157403.
77. Schuller, J.A.; Zia, R.; Taubner, T.; Brongersma, M.L. Dielectric metamaterials based on electric and magnetic resonances of silicon carbide particles. *Phys. Rev. Lett.* **2007**, *99*, 107401.
78. Ahmadi, A.; Mosallaei, H. Physical configuration and performance modeling of all-dielectric metamaterials. *Phys. Rev. B* **2008**, *77*, 045104.
79. Ma, Y.G.; Zhao, L.; Wang, P.; Ong, C.K. Fabrication of negative index materials using dielectric and metallic composite route. *Appl. Phys. Lett.* **2008**, *93*, 184103.
80. Vendik, O.G.; Gashinova, M.S. Artificial double negative (DNG) media composed by two different dielectric sphere lattices embedded in a dielectric matrix. *Proc. Eur. Microw. Conf.* **2004**, *34*, 1209–1212.
81. Lepetit, T.; Akmansoy, E.; Ganne, J.P. Experimental measurement of negative index in an all-dielectric metamaterial. *Appl. Phys. Lett.* **2009**, *95*, 121101.
82. Vendik, I.; Odit, M.; Kozlov, D. 3D metamaterials based on a regular array of resonant dielectric inclusions. *Radioengineering* **2009**, *18*, 111–116.
83. Zhao, Q.; Kang, L.; Du, B.; Zhao, H.; Xie, Q.; Huang, X.; Li, B.; Zhou, J.; Li, L. Experimental demonstration of isotropic negative permeability in a three-dimensional dielectric composite. *Phys. Rev. Lett.* **2008**, *101*, 027402.
84. Zhao, Q.; Du, B.; Kang, L.; Zhao, H.J.; Xie, Q.; Li, B.; Zhang, X.; Zhou, J.; Li, L.T.; Meng, Y.G.; Tunable negative permeability in an isotropic dielectric composite. *Appl. Phys. Lett.* **2008**, *92*, 051106.
85. Vynck, K.; Felbacq, D.; Centeno, E.; Căbuz, A.I.; Cassagne, D.; Guizal, B. All-dielectric rod-type metamaterials at optical frequencies. *Phys. Rev. Lett.* **2009**, *102*, 133901.
86. Gaillot, D.P.; Croënne, C.; Lippens, D. An all-dielectric route for terahertz cloaking. *Opt. Express* **2008**, *16*, 3986–3992.
87. Fedotov, V.A.; Mladyonov, P.L.; Prosvirnin, S.L.; Zheludev, N.I. Planar electromagnetic metamaterial with a fish scale structure. *Phys. Rev. E* **2005**, *72*, 036603.
88. Fedotov, V.A.; Rogacheva, A.V.; Prosvirnin, S.L.; Mladyonov, P.L.; Zheludev, N.I. Mirror that does not change the phase of reflected waves. *Appl. Phys. Lett.* **2006**, *88*, 091119.
89. Powell, C.J.; Swan, J.B. Effect of oxidation on the characteristic loss spectra of aluminium and magnesium. *Phys. Rev.* **1960**, *118640*, 643.
90. Sanders, R.W.; Belanger, R.M.; Motokawa, M.; Jaccarino, V.; Rezende, S.M. Far-infrared laser study of magnetic polaritons in FeF<sub>2</sub> and Mn impurity mode in FeF<sub>2</sub>:Mn. *Phys. Rev. B* **1981**, *23*, 1190.
91. Remer, L.; Lüthi, B.; Sauer, H.; Geick, R.; Camley, R.E. Nonreciprocal optical reflection of the uniaxial antiferromagnet MnF<sub>2</sub>. *Phys. Rev. Lett.* **1986**, *56*, 2752.
92. Liu, H.; Genov, D.A.; Wu, D.M.; Liu, Y.M.; Steele, J.M.; Sun, C.; Zhu, S.N.; Zhang, X. Magnetic plasmon propagation along a chain of connected subwavelength resonators at infrared frequencies. *Phys. Rev. Lett.* **2007**, *97*, 243902.
93. Linden, S.; Decker, M.; Wegener, M. Model system for a one-dimensional magnetic photonic crystal. *Phys. Rev. Lett.* **2006**, *97*, 083902.

94. Wang, S.M.; Li, T.; Liu, H.; Wang, F.M.; Zhu, S.N.; Zhang, X. Magnetic plasmon modes in periodic chains of nanosandwiches. *Opt. Express* **2008**, *16*, 3560.
95. Gollub, J.N.; Smith, D.R.; Vier, D.C.; Perram, T.; Mock, J.J. Experimental characterization of magnetic surface plasmons on metamaterials with negative permeability. *Phys. Rev. B* **2005**, *71*, 195402.
96. Pendry, J.B.; Schurig, D.; Smith, D.R. Controlling electromagnetic fields. *Science* **2006**, *312*, 1780–1782.
97. Liu, R.; Ji, C.; Mock, J.J.; Chin, J.Y.; Cui, T.J.; Smith, D.R. Broadband ground-plane cloak. *Science* **2009**, *323*, 366–369.
98. Ergin, T.; Stenger, N.; Brenner, P.; Pendry, J.B.; Wegener, M. Three-dimensional invisibility cloak at optical wavelengths. *Science* **2010**, *328*, 337–339.
99. Lai, Y.; Chen, H.Y.; Zhang, Z.Q.; Chan, C.T. Complementary media invisibility cloak that cloaks objects at a distance outside the cloaking shell. *Phys. Rev. Lett.* **2009**, *102*, 093091.
100. Lai, Y.; Ng, J.; Chen, H.Y.; Han, D.Z.; Xiao, J.J.; Zhang, Z.Q.; Chan, C.T. Illusion optics: The optical transformation of an object into another object. *Phys. Rev. Lett.* **2009**, *102*, 253902.
101. Lukin, M.D.; Imamoglu, A. Controlling photons using electromagnetically induced transparency. *Nature* **2001**, *413*, 273–276.
102. Zhao, X.P.; Luo, W.; Huang, J.X.; Fu, Q.H.; Song, K.; Cheng, X.C.; Luo, C.R. Trapped rainbow effect in visible light left-handed heterostructures. *Appl. Phys. Lett.* **2009**, *95*, 071111–071113.
103. Zhang, S.; Genov, D.A.; Wang, Y.; Liu, M.; Zhang, X. Plasmon-induced transparency in metamaterials. *Phys. Rev. Lett.* **2008**, *101*, 047401.
104. Liu, N.; Langguth, L.; Weiss, T.; Kästel, J.; Fleischhauer, M.; Pfau, T.; Giessen, H. Plasmonic analogue of electromagnetically induced transparency at the Drude damping limit. *Nat. Mater.* **2009**, *8*, 758–762.
105. Liu, N.; Weiss, T.; Mesch, M.; Langguth, L.; Eigenthaler, U.; Hirscher, M.; Sönnichsen, C.; Giessen, H. Plasmonic metamaterial analogue of electromagnetically induced transparency for plasmonic sensing. *Nano Lett.* **2010**, *10*, 1103–1107.
106. Tsakmakidis, K.L.; Hermann, C.; Klaedtke, A.; Jamois, C.; Hess, O. Surface plasmon polaritons in generalized slab heterostructures with negative permittivity and permeability. *Phys. Rev. B* **2006**, *73*, 085104.
107. Lu, W.T.; Savo, S.; Casse, B.D.F.; Sridhar, S. Slow microwave waveguide made of negative permeability metamaterials. *Microw. Opt. Tech. Lett.* **2009**, *51*, 2705–2709.
108. Tsakmakidis, K.L.; Klaedtke, A.; Aryal, D.P.; Jamois, C.; Hess, O. Single-mode operation in the slow-light regime using oscillatory waves in generalized left-handed heterostructures. *Appl. Phys. Lett.* **2006**, *89*, 201103.
109. Rawal, S.; Sinha, R.K.; De La Rue, R.M. Slow light miniature devices with ultra-flattened dispersion in silicon-on-insulator photonic crystal. *Opt. Express* **2009**, *17*, 13315–13325.
110. Oskooi, A.F.; Joannopoulos, J.D.; Johnson, S.G. Zero-group-velocity modes in chalcogenide holey photonic-crystal fibers. *Opt. Express* **2009**, *17*, 10082–10090.
111. Vukovic, S.M.; Aleksic, N.B.; Timotijevic, D.V. Guided modes in left-handed waveguides. *Opt. Commun.* **2008**, *281*, 1500–1509.

112. Lai, H.M.; Kwok, C.W.; Loo, Y.W.; Xu, B.Y. Energy-flux pattern in the Goos-Hanchen effect. *Phys. Rev. E* **2000**, *62*, 7330–7339.
113. Berman, P.R. Goos-Hanchen shift in negatively refractive media. *Phys. Rev. E* **2002**, *66*, 3.
114. Gan, Q.Q.; Ding, Y.J.; Bartoli, F.J. “Rainbow” trapping and releasing at telecommunication wavelengths. *Phys. Rev. Lett.* **2009**, *102*, 4.

© 2011 by the authors; licensee MDPI, Basel, Switzerland. This article is an open access article distributed under the terms and conditions of the Creative Commons Attribution license (<http://creativecommons.org/licenses/by/3.0/>).